Eidgenössische Technische Hochschule Zürich
Swiss Federal Institute of Technology Zurich

SED
Schweizerischer Erdbebendienst
Swiss Seismological Service

Report on site characterization

Hämikon, Switzerland (HAMIK)

Poggi Valerio, Ulrike Kleinbrod, Donat Fäh

Last modified - 23 / 12 / 2014

1. Introduction

In the framework of the NAGRA seismic network project, an array measurement of the ambient vibration wave-field was performed at the location of the SED borehole station HAMIK (Hämikon, Switzerland). The scope of the survey is the seismic characterization of the area surrounding the installation (**Figure 1**), which consists in a short period borehole sensor at about 100m, and a collocated strong motion seismometer at the surface, with a high-resolution digitizer (Taurus 24Bit @200sps). Ambient vibration analysis has been used to infer the characteristics of the underground structure of the site, with special regard to the one-dimensional shear-wave velocity. Such profile was later compared with the results from active seismic measurements and used to assess the local seismic response of the station.

For the analysis, different spectral analysis techniques were implemented, consisting in both single and array methods, which are listed below:

- Time-frequency wavelet analysis
- Power-spectral density estimation
- Conventional horizontal to vertical spectral ratios
- Directional horizontal to vertical spectral ratios
- Wavelet polarization analysis
- Three-component high-resolution f-k analysis.

The results of all these analyses conformed to the definition of the final velocity model. In the following, the main results of these investigations are summarized and a final interpretation of the velocity profile is given. From this interpretation, engineering parameters are finally derived, e.g. the Qwl-Vs average velocity, VsZ (including Vs30) and the seismic amplification from the analytical SH-transfer function of the one-dimensional soil column.

2. Survey description

To characterize the seismic response of the site, an array measurement of ambient vibration was performed on 25/02/2014 (**Figure 1**). The array consists of three concentric measuring configurations (called “rings”, R1, R2 and R3) of 14 sensors each and increasing diameter (about 40m, 120m and 200m respectively). The three configurations were planned to partially overlap, with the aim of providing a continuous frequency resolution between the geometries. Configuration R1 recorded for a total of 35m, while configuration R2 for 45m and R2 for 1h15m. The differences in the recording length are due to the different resolution characteristics of the three geometries. As a general rule, larger arrays require longer recording time to produce a reasonable statistics of the ambient vibration processing results. Satisfactory results were obtained from the analysis of all the geometries. For the larger configuration, a penetration depth of 100~150m was initially expected.

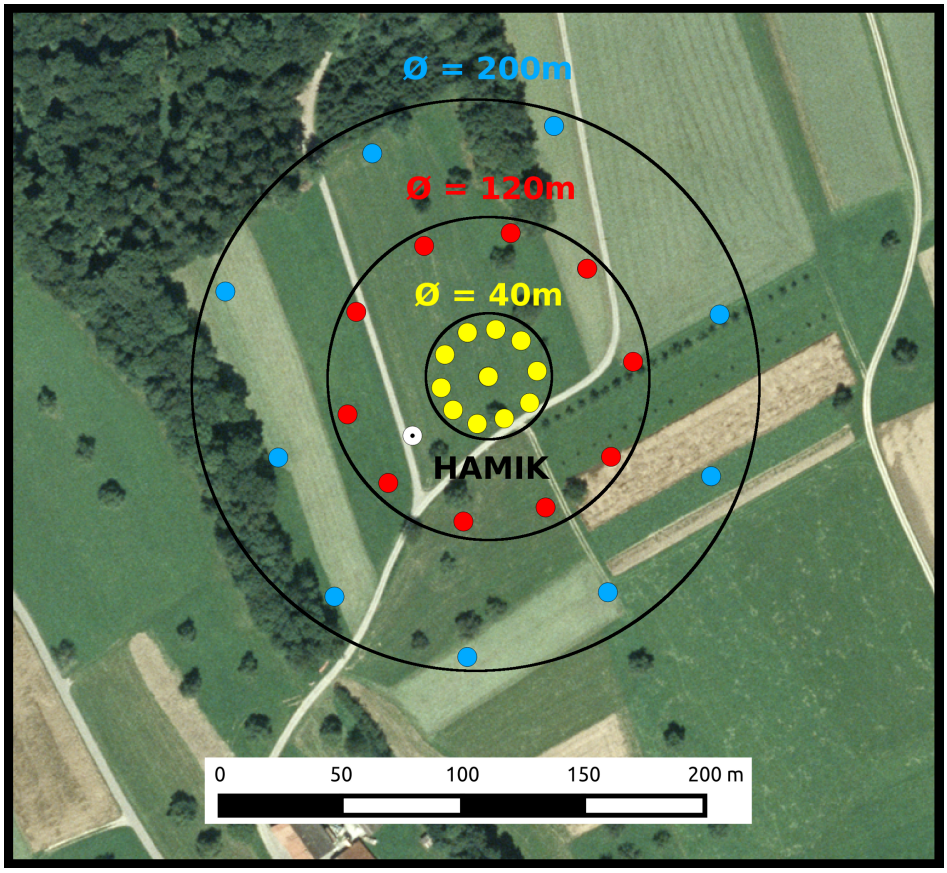

Figure 1 - *Location of the ambient vibration array survey performed in Hämikon, (SED station HAMIK) on 25/02/2014. Three concentric configurations of increasing diameter were implemented (named R1, R2 and R3). Location of the permanent station is shown with a white dot, between configurations R1 an R2.*

3. Soil type, topography and geology

The array has been set in open field conditions, in a rural area (**Figure 1**, **Figure 3**). The influence of buildings and anthropogenic disturbances is virtually negligible. Array sensors have been deployed on free soil. Good coupling with the ground was assured by means of digging small holes at the sensor's places, and by using a special support (*Trihedron*®) that facilitates the leveling of the device even for difficult soil conditions. The measurement area was located on a small ridge, roughly aligned N-S. However, maximum elevation difference between sensor locations was less than 5m, and therefore no topographic correction was necessary before processing.

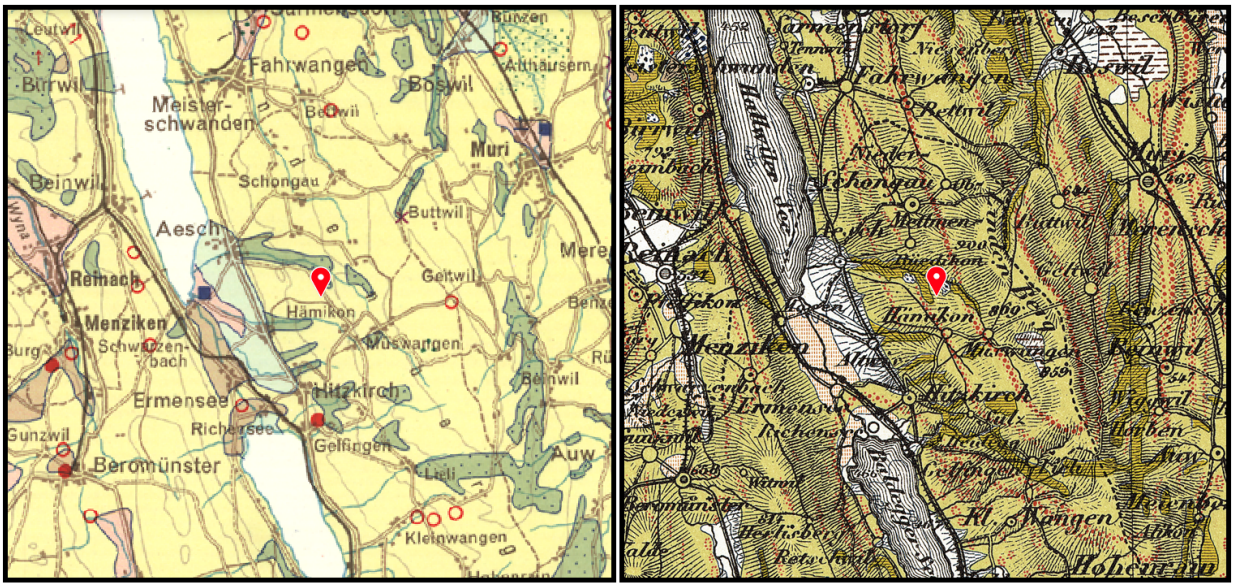

Figure 2 - *Geological map of the measuring area, in the surroundings of Hämikon (reproduced from Swisstopo, "Geologische Generalkarte der Schweiz" to the right, "Geotechnics and rocks" to the left, modified). In red the approximate location of the permanent station HAMIK.*

From the geological points of view (**Figure 2**) the target area is located on a small hill on the Molasse basin. The surface morphology is considerably smooth and modeled by the action of glaciers during the Pleistocene. The measuring area is visibly surrounded by moranic deposits, clearly identifiable from the surface morphology and confirmed by the geological map of the area. The Molassic bedrock is never exposed across the area (a variable-thick cover of quaternary soil material is generally present). The bedrock probably consists of marl and consolidated sandstone with layers of different texture and granulometry, from very fine sand and silt to occasionally conglomerate. Such site can be classified as of rock ground-type A.

4. Weather conditions

The weather conditions were optimal and stable during the whole measurement, with no precipitations, no wind and an average temperature of 5 degrees.

Figure 3 - *Overview of the measurement area at the location of the array central station.*

5. Acquisition equipment

Each acquisition point within the array consisted of a three components seismometer (Lennartz 3C with 5s eigenperiod) and a 24 bit data logger (Quanterra Q330). Synchronization between stations was assured by standard GPS, while a more accurate differential GPS (Leica Viva system) was used to precisely locate the sensor's coordinates with a tolerance of less than 5cm.

6. Pre-processing and preliminary data-quality control

The three-component recording has been filtered prior to analysis using a band-pass 6th order causal Butterworth filter with corners at 0.2Hz and 50Hz. Although it is not a strict requirement for spectral analysis techniques, such filtering was applied in order to facilitate the preliminary visual inspection of the noise traces and to evaluate the coherency of the wave-field (**Figure 4**). Such procedure gives essential information for the subsequent interpretation of the f-k analysis results.

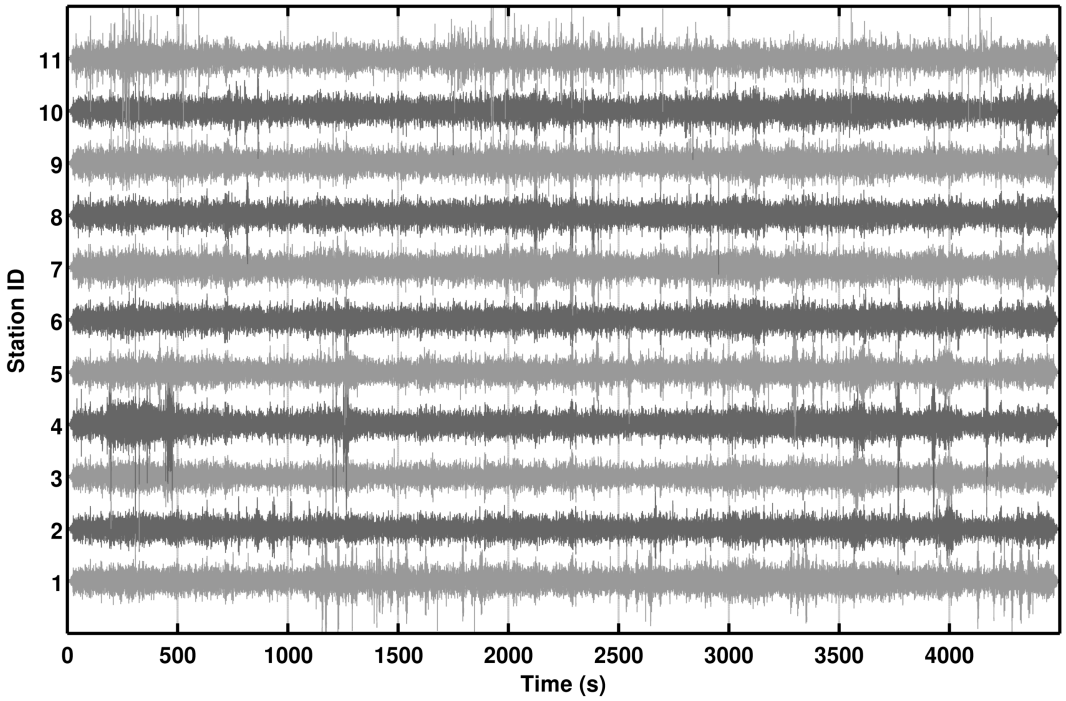

Figure 4 - *Inspection of the useful part of the ambient vibration recording of the Hämikon array (here ring configuration R3). No strong transients were present during the acquisition, which resulted in an overall good quality of the recordings.*

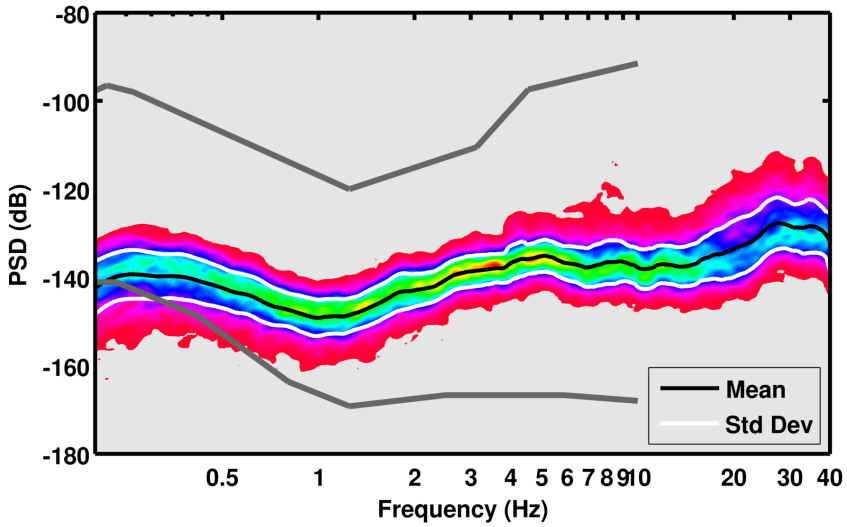

Figure 5 - *Power spectral density (PSD) computed for 1h15m recording at the central station of the array configuration R3, horizontal direction N-S. Similar results were obtained for the other stations of the array. In gray lines are the minimum and the maximum bounds of the USGS noise model, for comparison.*

To assess the quality of the ambient vibration recordings, spectral analysis was subsequently performed. Because of the stochastic nature of the ambient vibration wave-field, a statistical approach has to be used, such as the estimation of the power spectral density (*PSD*). This approach is useful to evaluate the average energy level of the recordings in the analyzed frequency range, and to access the presence of spurious spectral peaks, which might be related to human activity (machinery, pumps).

By inspecting the PSD of all the three-component recordings of the array in the range between 0.5 and 40Hz, is found that the average energy level of the spectrum is overall very low, well within the minimum and maximum bounds of the USGS noise model (**Figure 5**). No relevant peaks of anthropogenic origin, which might affect the processing, are identified.

Complementary to the aforementioned statistical methods, a spectral decomposition approach is more suitable to assess the stationarity of the ambient vibration wave-field over time. The wavelet time-frequency analysis was then performed over the whole recording time. From such analysis (**Figure 6**) an overall stability of the ambient-vibration wave-field over time is evident.

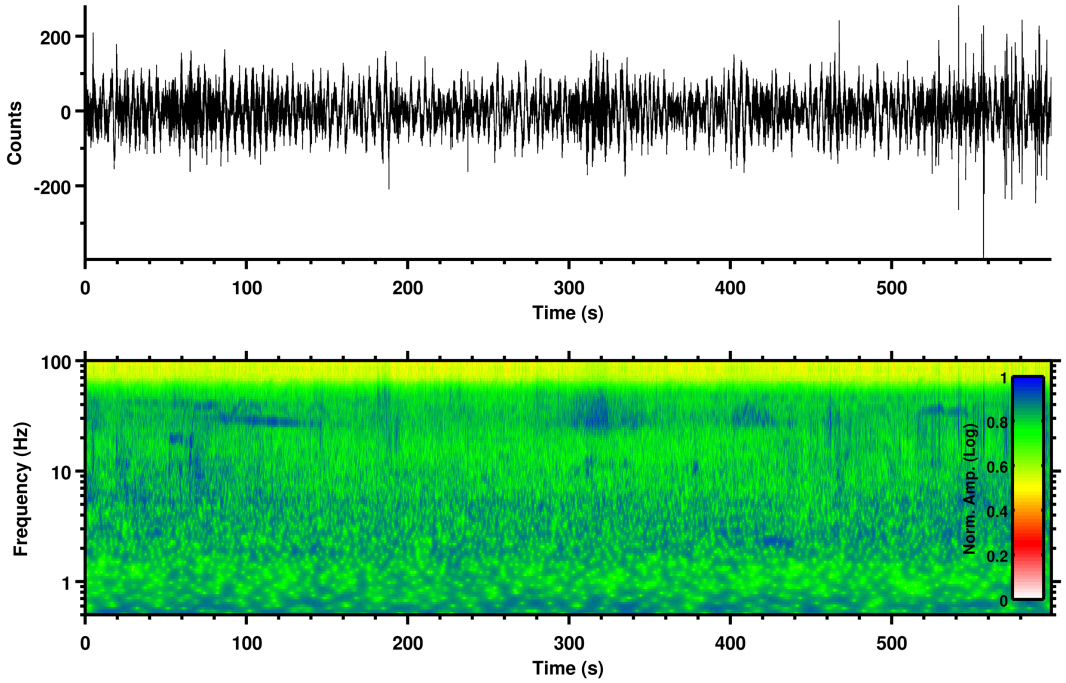

Figure 6 - *Example of spectrogram from 600s of recording of the central station (HMK11) of the array configuration A2. A part from few very localized transients, no sign of persistent disturbances are visible on the whole spectrogram. For the analysis, the cosine wavelet is used (wavelet parameter = 12).*

7. Conventional H/V spectral ratios

The horizontal-to-vertical (H/V) Fourier spectral ratio is a technique widely used in seismic site characterization because of its ability to provide an estimate of the SH wave fundamental frequency of resonance (f_0) of the site. Other than that, H/V ratios are useful to provide information on the Rayleigh wave ellipticity function, which can be used in surface wave dispersion inversion procedures to constrain large velocity contrasts at depth. In this study, we use the H/V technique also to map the variability of the subsoil structure along the investigated area; this is necessary to verify the fulfillment of the 1D structure assumption, which is necessary for the f-k method applied later.

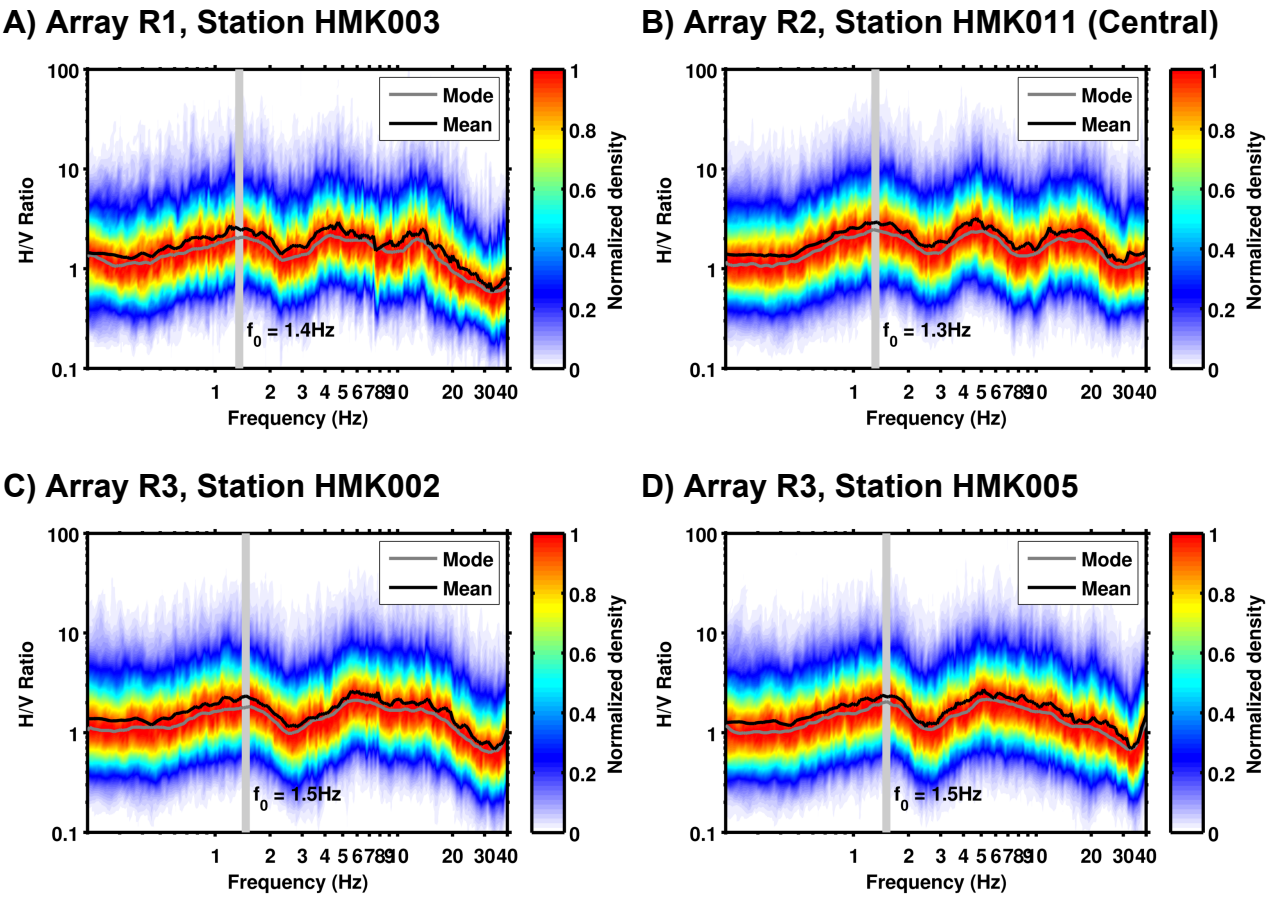

Figure 7 - *Example of H/V spectral ratios for the three concentric configurations R1, R2 and R3. The resonance frequency is indicated with a light gray line (~1.4Hz). An additional peak is visible at about 5~6Hz, more pronounced on those stations close to the center (in R1 and R2) and located on top of the small ridge.*

H/V spectral ratios have been computed for all the recordings at each station of the array and separately for configurations R1, R2 and R3 (e.g. **Figure 7**). The behavior of the noise wave-field at the different stations location is comparable at low frequency (roughly < 6-8Hz), while the high frequency region shows more variability, within and between arrays. In average (**Figure 8**) spectral curves show a relatively stable low frequency peak (around 1.4Hz). Such maximum is likely induced by a change in lithology at depth, which causes a modest contrast of seismic impedance. The peak should be regarded as the fundamental resonance frequency of the site (f_0). A second peak is also present at about 5~6Hz, but not stable over all stations. Such peak, in particular, is more persistent on the inner configurations (R1 and R2), which are located on top of the ridge (the flat part). On stations close to the array center, an additional third peak is identified (~14Hz). The peak is however less visible on stations from the larger configuration (R3); such maximum is likely induced by the Quaternary soil cover, which can be very heterogeneous over the measuring area. The behavior of the site can be considered laterally homogeneous for the f-k analysis.

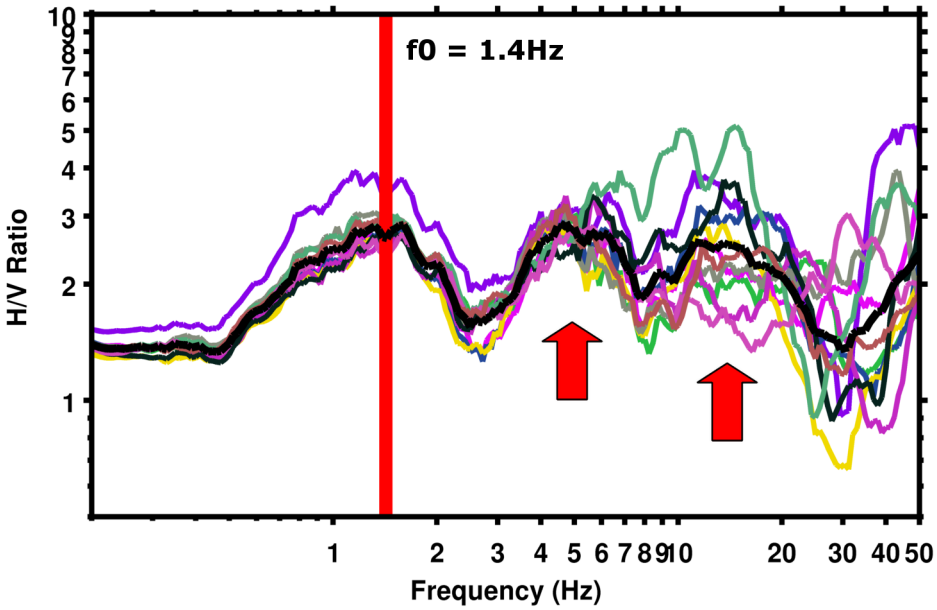

Figure 8 - *Comparison of the H/V spectral ratio curves of all the stations of the array (in this example for the array configuration R3). The curves are stable up to at least 8Hz, confirming the lateral homogeneity of the underlying bedrock velocity structure of the site. A low frequency peak is visible at about 1.4Hz. Two additional peaks can be identified at 5-6Hz and ~14Hz.*

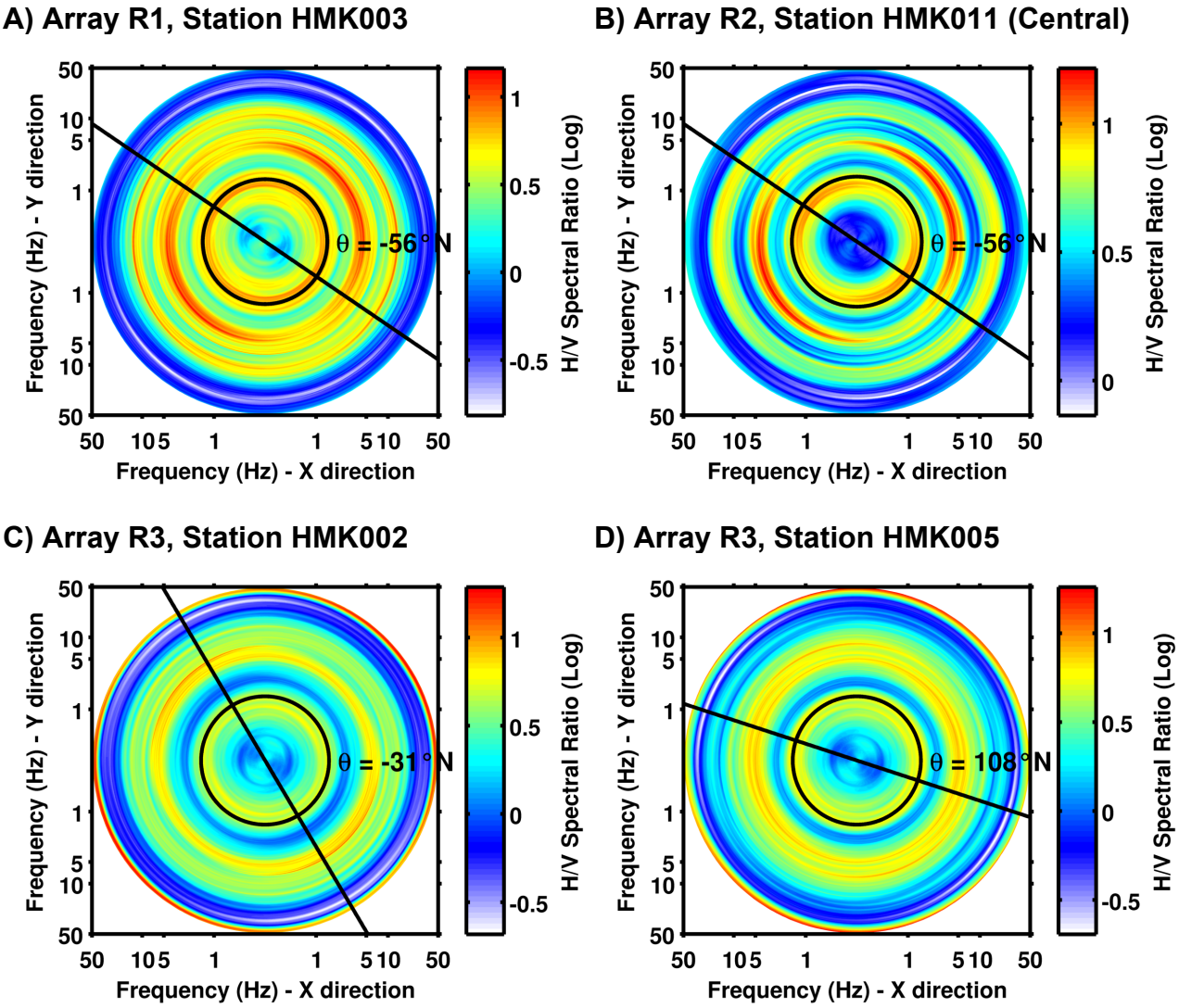

Figure 9 - *Example of directional H/V spectral ratios for the three concentric configurations R1, R2 and R3. The low frequency resonance peak (f_0) is preferentially (but not always) aligned roughly NW-SE (along the ridge axis). Also the second peak (5~6Hz) shows a nearly constant polarization direction (approx. ~60°N), but only for those stations close to the array center (R1 and R2, on top of the ridge).*

8. Directional analysis

The computation of directional H/V spectral ratio or polarization analysis is useful to reveal asymmetries in the ambient vibration wave-field. Different effects can induce such a behavior: 2D/3D structure, topographic effects or a non-homogeneous distribution of the noise sources. If a strong directionality is found by the analysis, it is generally recommended to carry out further investigations to properly address the origin of polarization. By processing the directional H/V ratios at all the recording stations of the array (e.g. **Figure 9**) it is possible to observe a moderate directionality of the identified resonance peaks. The fundamental frequency shows a preferential (but not strict) alignment along direction NW-SE, visible on most but not all the stations of the three geometries. Such direction is consistent with the approximate direction of the topographic ridge. Conversely, the second peak shows evidences of strong directionality toward NE-SW (~60°N), but only on those stations close to the array center (on the hilltop, e.g. **Figure 9**A, B); at the edges (stations of configuration R3) such directionality is lost (e.g. **Figure 9**C, D). This behavior is likely induced by the local geology.

The results of the H/V directional analysis are only partially confirmed by applying the wavelet polarization analysis technique (Burjanek et al., 2008). Here, the particle motion shows to be mostly elliptical, with just a weak polarization at the resonance frequencies (**Figure 10**). The frequency corresponding to f_0 shows nearly no (or very weak) directionality on azimuth (**Figure 11**A), but a strong directionality on the dip (**Figure 11**B). The second peak has weak directionality, but consistent with H/V spectral ratio.

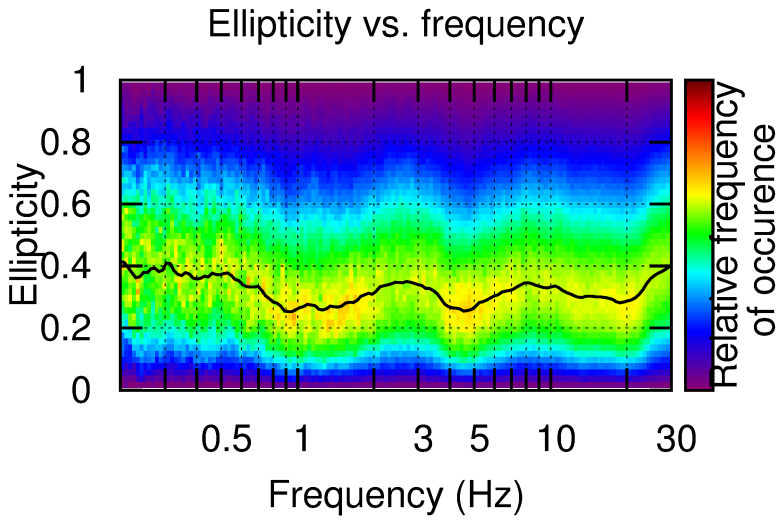

Figure 10 - *Ellipticity of the particle motion from wavelet-based polarization analysis at the central station of the array (HMK11).*

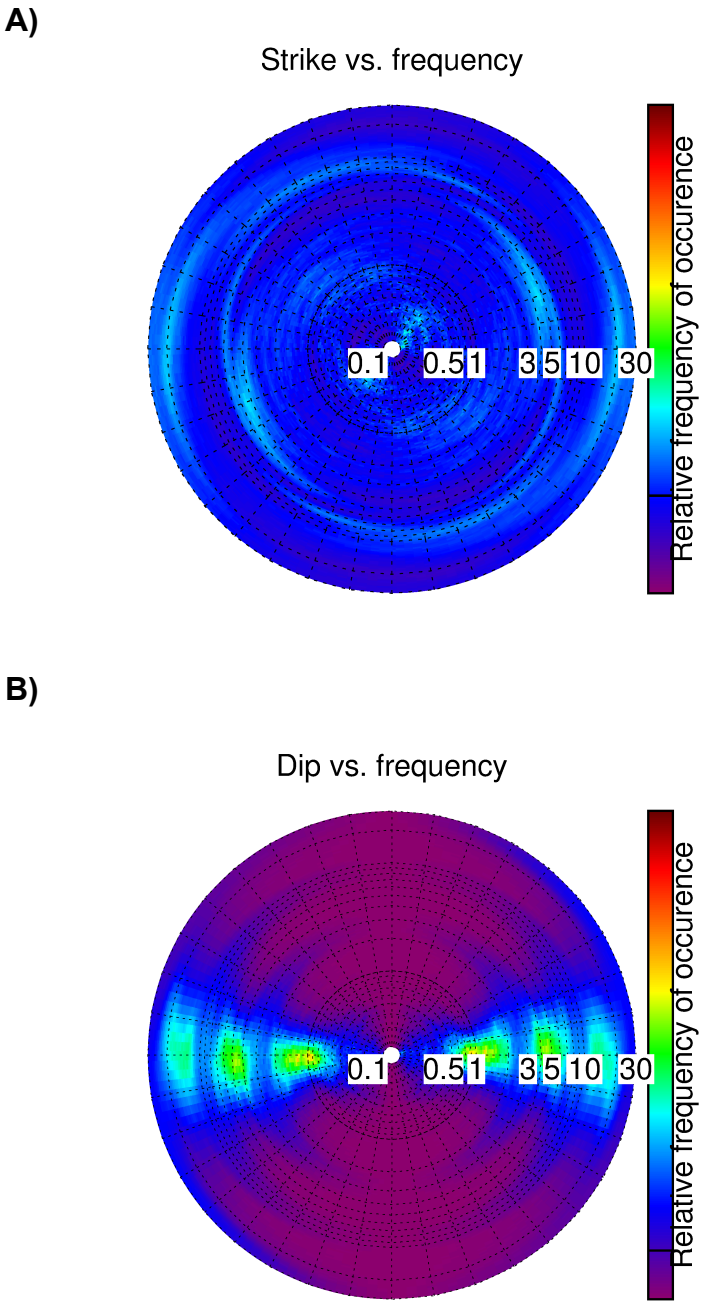

Figure 11 - *Directionality of the particle motion from wavelet-based polarization analysis (dip direction in B, strike in A) at the central station of the array (HMK11).*

9. Three-component f-k analysis

The frequency-wavenumber analysis is a spectral technique based on seismic array recordings that allows retrieving direction and dispersion characteristics of the surface waves. We apply this technique to three-component ambient vibration recordings using a modification of the high-resolution method of Capon (1969) as described in Poggi et al. (2010). Using all the three-components of motion gives the possibility to retrieve information about the propagation of the Rayleigh waves (vertical and radial processing direction) as well as of the Love waves (transversal direction).

As in the case of the previous methods, the ambient vibration recordings are treated statistically by subdividing the traces in sub-windows. For each consecutive window a separated f-k analysis is performed, and the results are then averaged over the whole recording, increasing the robustness of the final estimation.

A) Ring 2, 2-5Hz

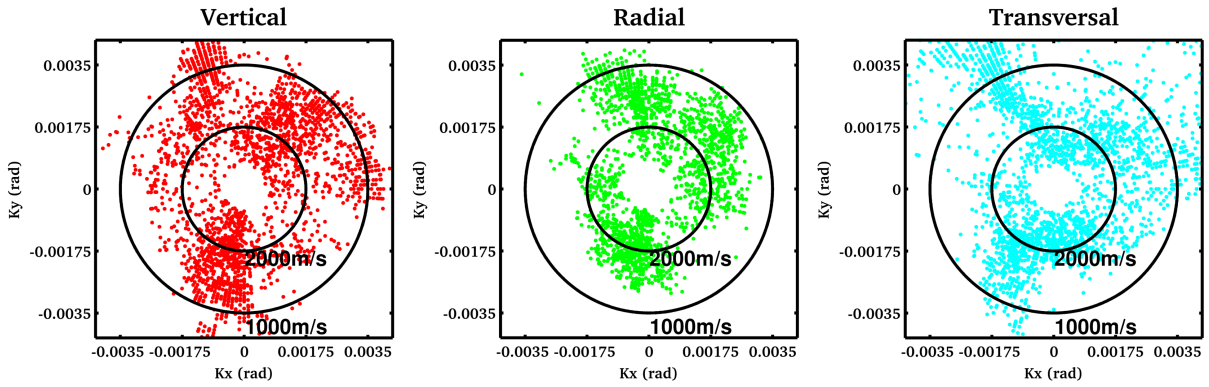

B) Ring2, 5-10Hz

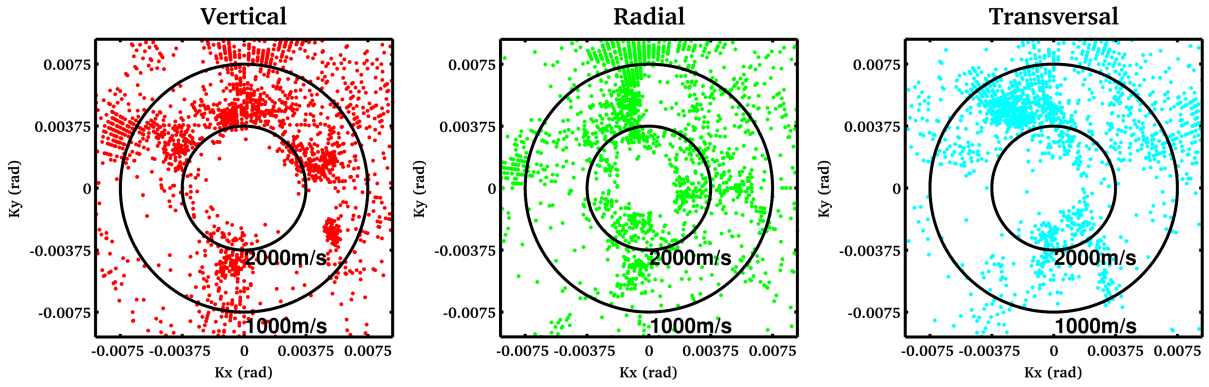

Figure 12 - *Example of distribution of noise sources in the low (2-6Hz) and intermediate frequency range (5-10Hz) obtained from three-component f-k analysis. The source distribution is irregular but not strictly directional on all the propagation components.*

As first step, from the f-k analysis it is possible to assess the noise source azimuthal distribution over different ranges of frequencies (e.g. **Figure 12**) separately for the vertical, the radial and the transversal direction of polarization. From the analysis of the two geometries A1 and A2, source distribution appears to be quite inhomogeneous in all the components, without nevertheless displaying a clear directional pattern.

As a second step, the surface-wave dispersion curves are extracted by visual inspection and manual picking of the f-k density plots (**Figure 13**, **Figure 14** and **Figure 15**), separately for the three polarization directions. Complementary results have been obtained for the three array configurations. In particular, Love wave dispersion can be well tracked in a broad frequency range (from 1.6Hz to about 18Hz) from R1 to R3; velocity estimates are also consistent between the different geometries. Rayleigh wave dispersion is of more difficult interpretation. Vertical and radial components from configurations R2 and R3 show a considerable discontinuity at about 4-5Hz. Dispersion function can then be interpreted in two ways. As first attempt, the discontinuity can be considered as the effect of a modal jump, leading to a two-mode interpretation (fundamental plus first higher). Alternatively, the whole dispersion can be addressed to a single mode (fundamental) with a minimum energy content at 4-5Hz due to velocity osculation with a higher mode. The first interpretation is not supported by inversion, showing clear incompatibility with Love wave dispersion. Conversely, the second interpretation results in good fitting of all available data (see next section). We therefore consider the single mode hypothesis as the more reliable.

A summary of all the identified modes from vertical, radial and transversal direction of propagation is presented in **Figure 16**, while the final interpretation of Rayleigh and Love wave dispersion pattern is in **Figure 17**, together with the results from an active seismic survey performed on the same location by the company *RoXplore*. Active surface wave analysis results (MASW) are compatible with our interpretation, extending the resolution at high frequencies and adding a Rayleigh wave higher mode to the interpretation model.

10. Inversion of the dispersion curves

The surface wave dispersion curves (Rayleigh and Love) obtained from the three-component f-k analysis of the ambient vibrations and the fundamental frequency of resonance (f_0) from average H/V spectral ratios are inverted to obtain an estimation of the velocity profile of the site (mainly S-wave velocity as function of depth, and to a lesser extend the P-wave velocity, due to the lower sensitivity). The analysis is performed using the software *Dinver* (www.geopsy.org), which implements a direct search approach (**Figure 18**) based on a conditional version of the neighborhood algorithm (Sambridge, 1999).

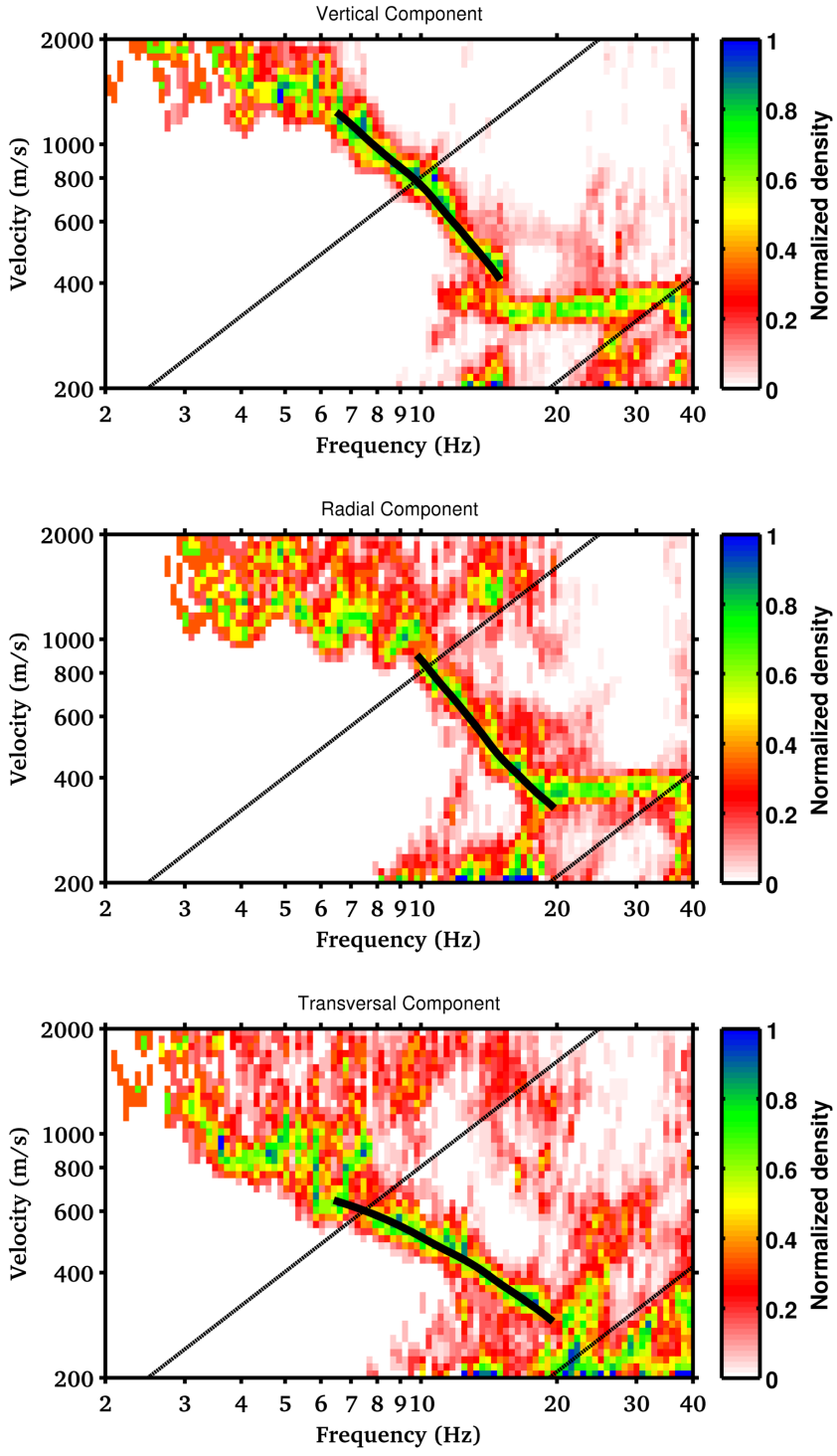

Figure 13 - *Density distribution of the surface wave signals obtained from the recording of the array configuration R1 using three-component f-k analysis. From top to bottom: Rayleigh vertical, Rayleigh radial and Love wave dispersion. In black the interpreted dispersion curves are given (manually selected).*

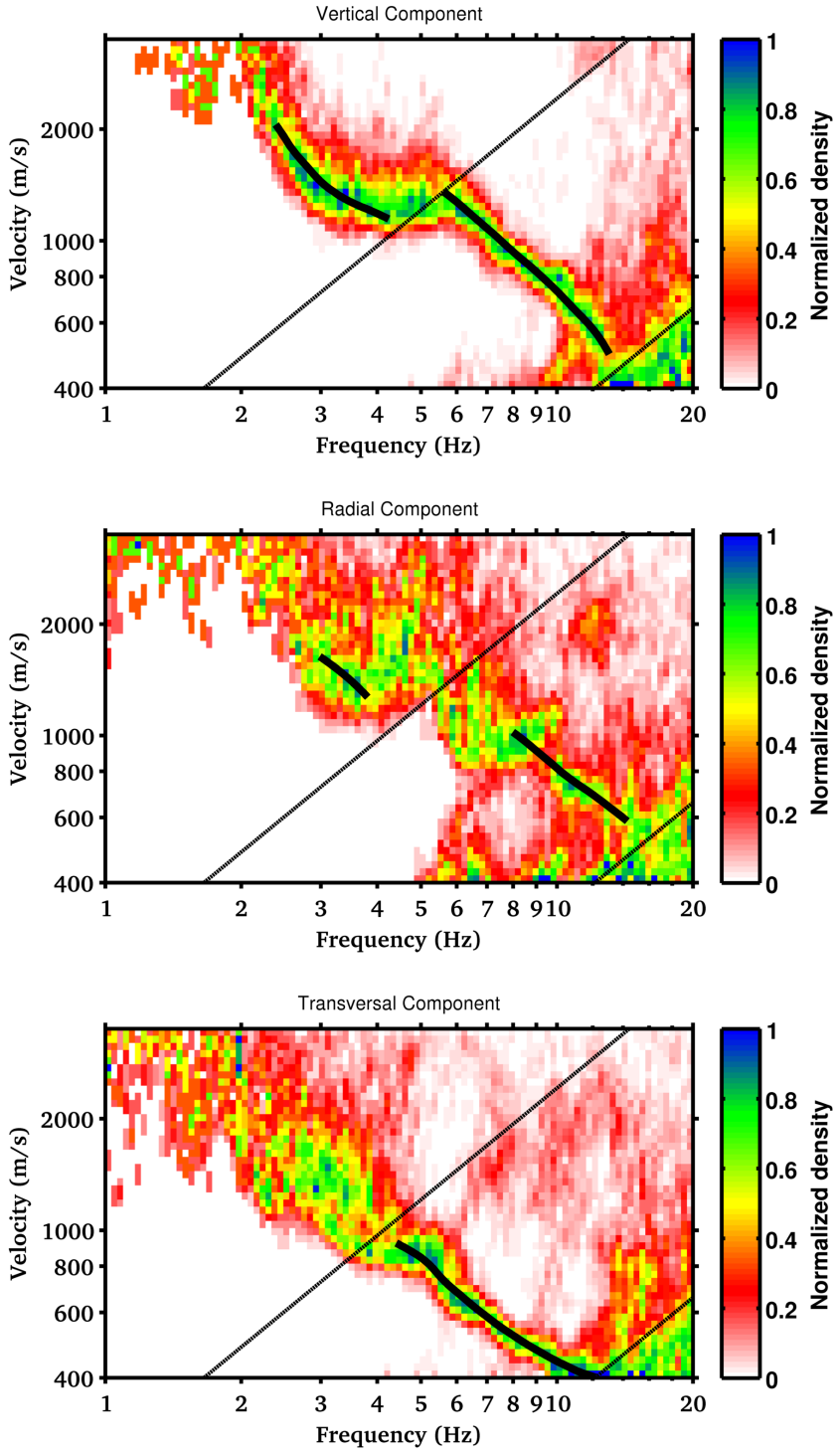

Figure 14 - *Density distribution of the surface wave signals obtained from the recording of the array configuration R2 using three-component f-k analysis. From top to bottom: Rayleigh vertical, Rayleigh radial and Love wave dispersion. In black the interpreted dispersion curves are given (manually selected).*

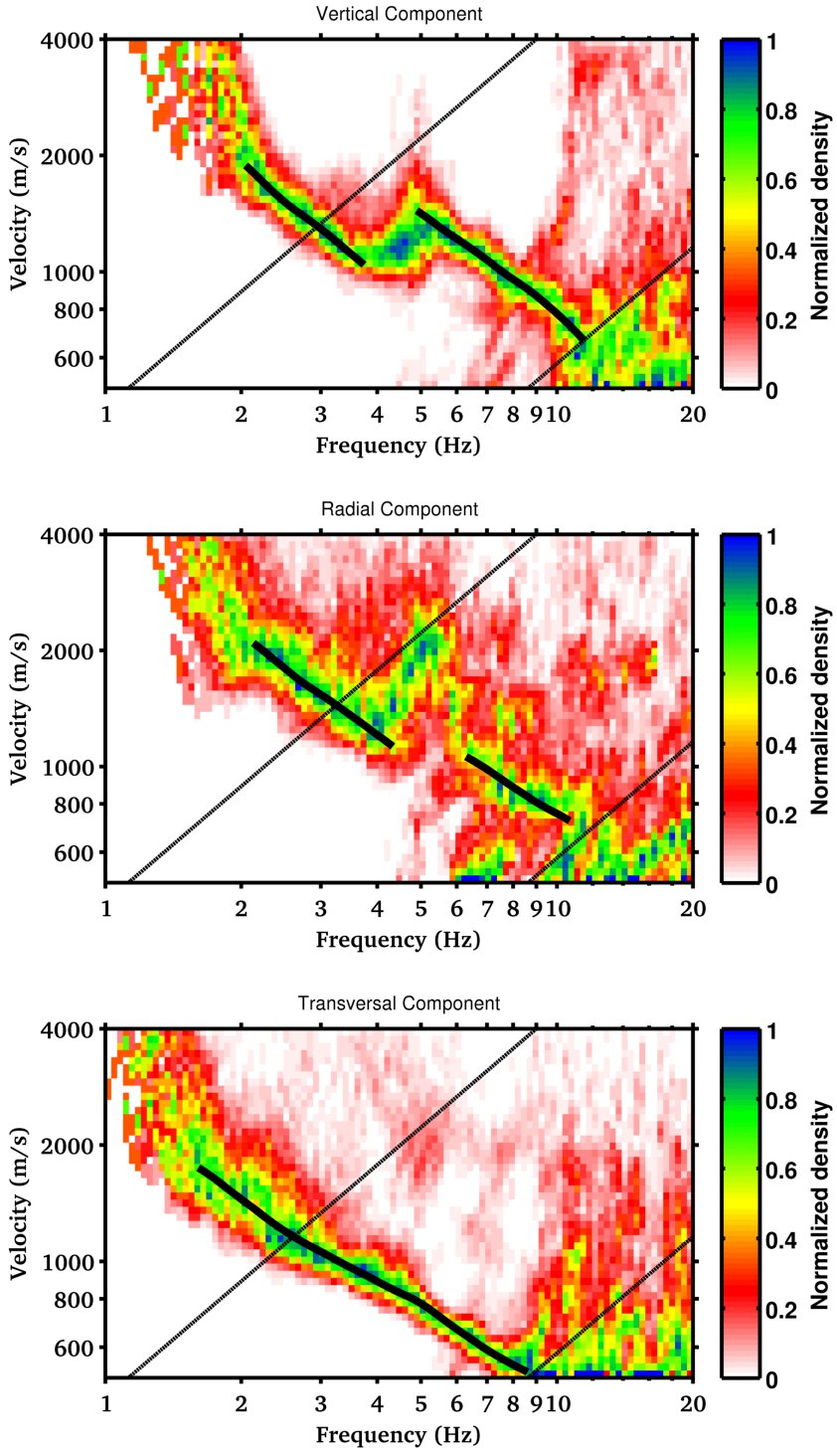

Figure 15 - *Density distribution of the surface wave signals obtained from the recording of the array configuration R3 using three-component f-k analysis. From top to bottom: Rayleigh vertical, Rayleigh radial and Love wave dispersion. In red the interpreted dispersion curves are given (manually selected).*

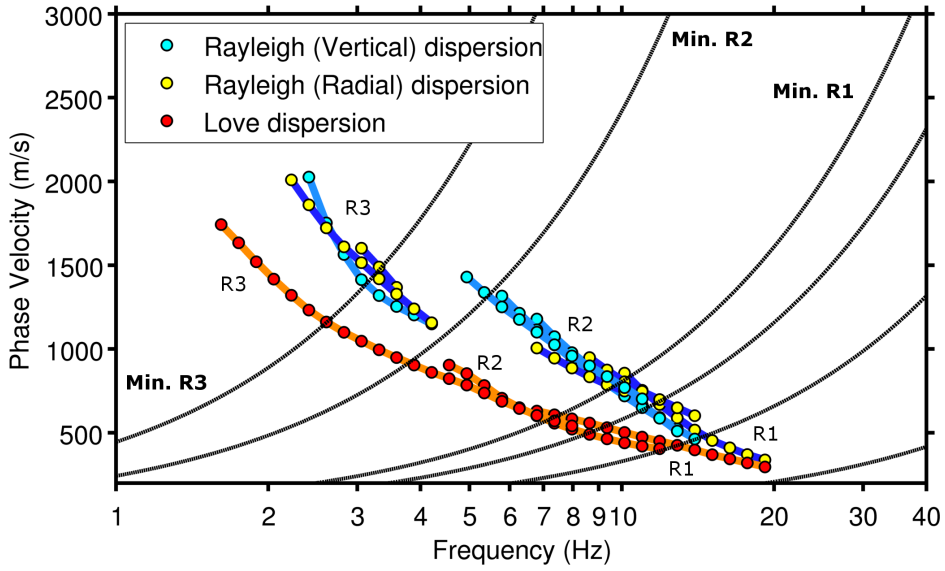

Figure 16 - *Summary of all dispersion curves obtained from three-component f-k analysis of the three array configurations R1, R2 and R3. Minimum and maximum resolution bounds from the two geometries are indicated with black solid lines.*

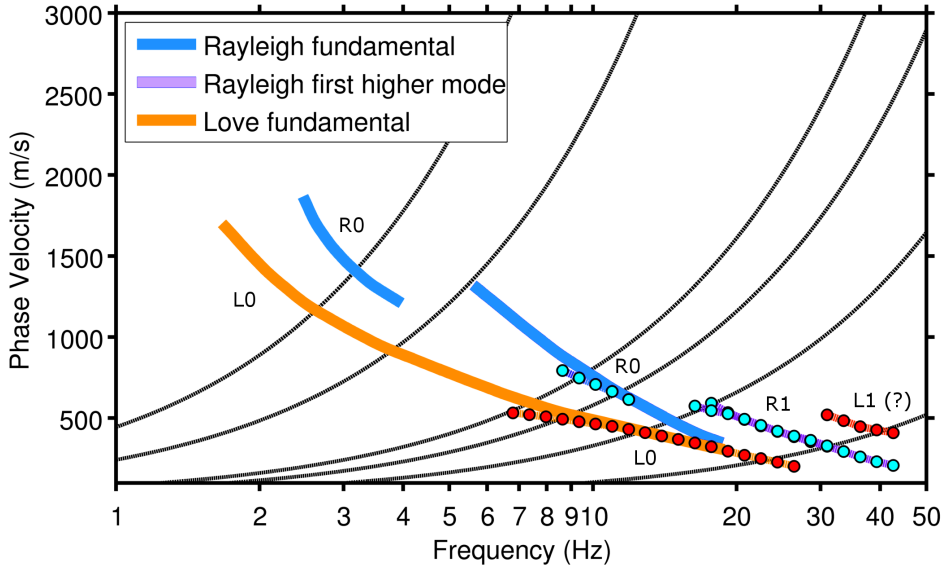

Figure 17 - *Final interpretation of the Rayleigh and Love dispersion curves for HAMIK, including the results from active surface wave analysis (MASW, with dots). Minimum and maximum resolution bounds from the full array are indicated with black solid lines.*

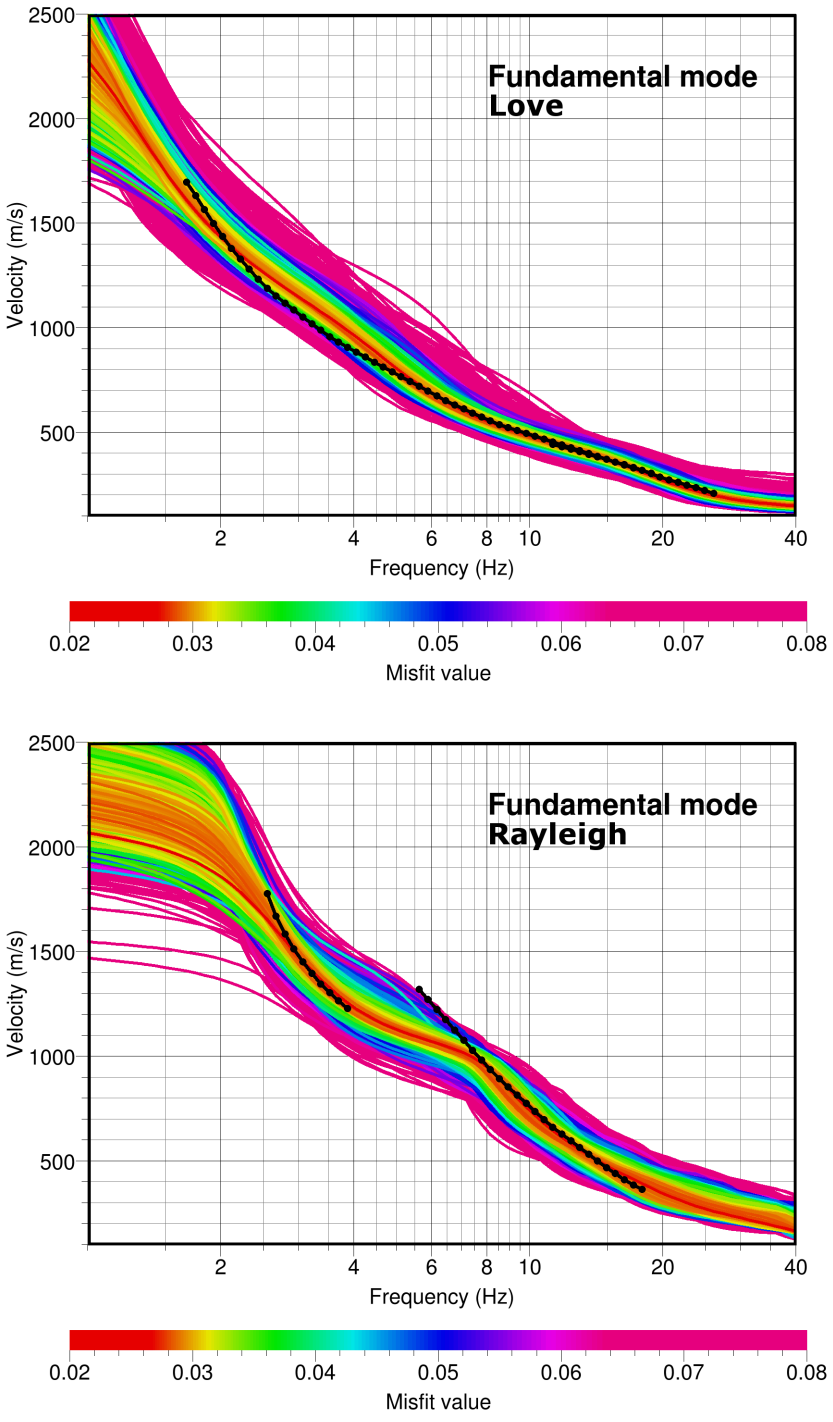

Figure 18 - *Example of fitting the surface dispersion data within the global optimization procedure. Different colors represent different misfit between the observed (in black) and the modeled dispersion curves during the search.*

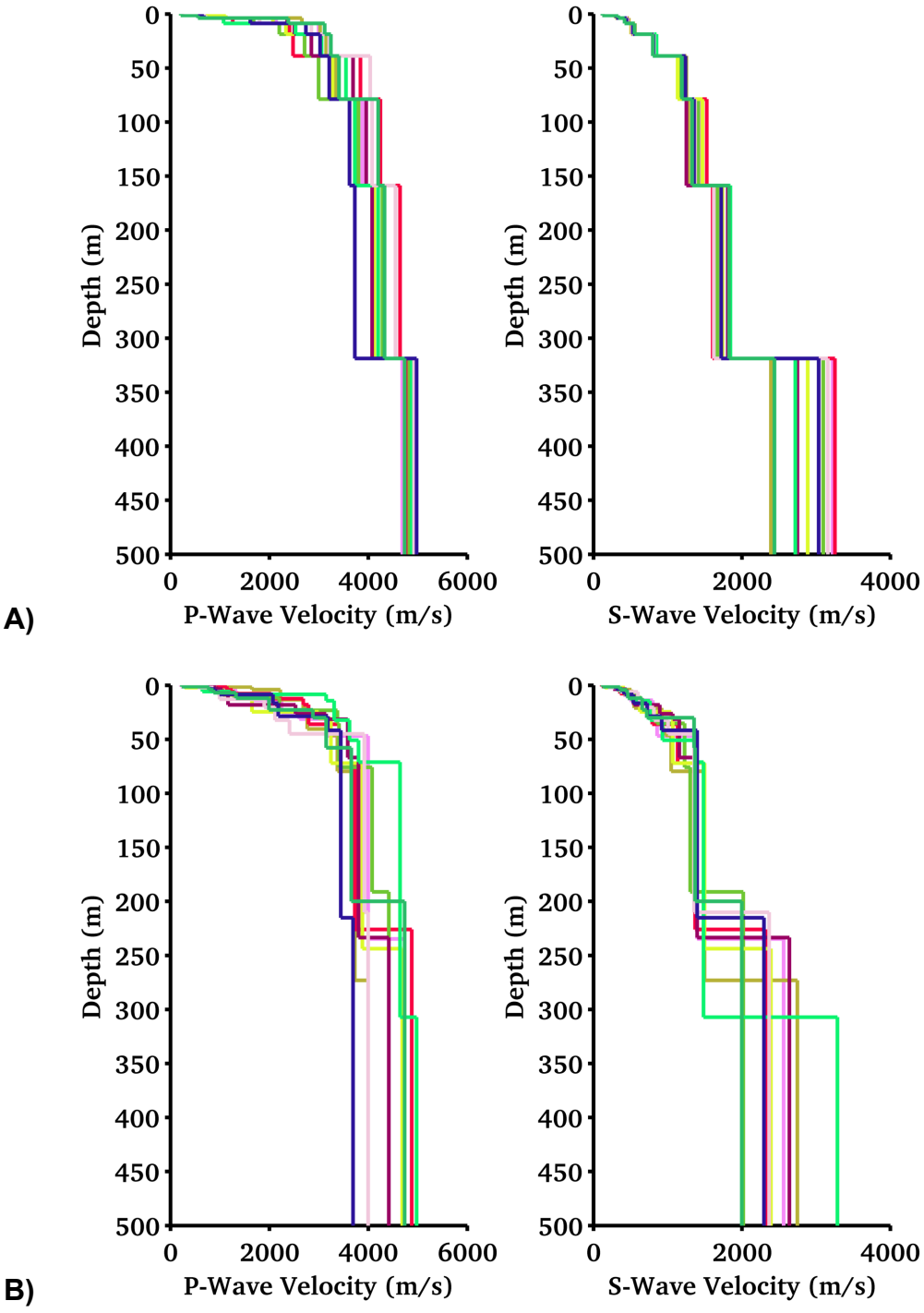

Figure 19 - *Collecting the best fitting models from the ten separated inversion runs using the free-layers (A, top) and fixed-layers (B, bottom) parameterization schemes.*

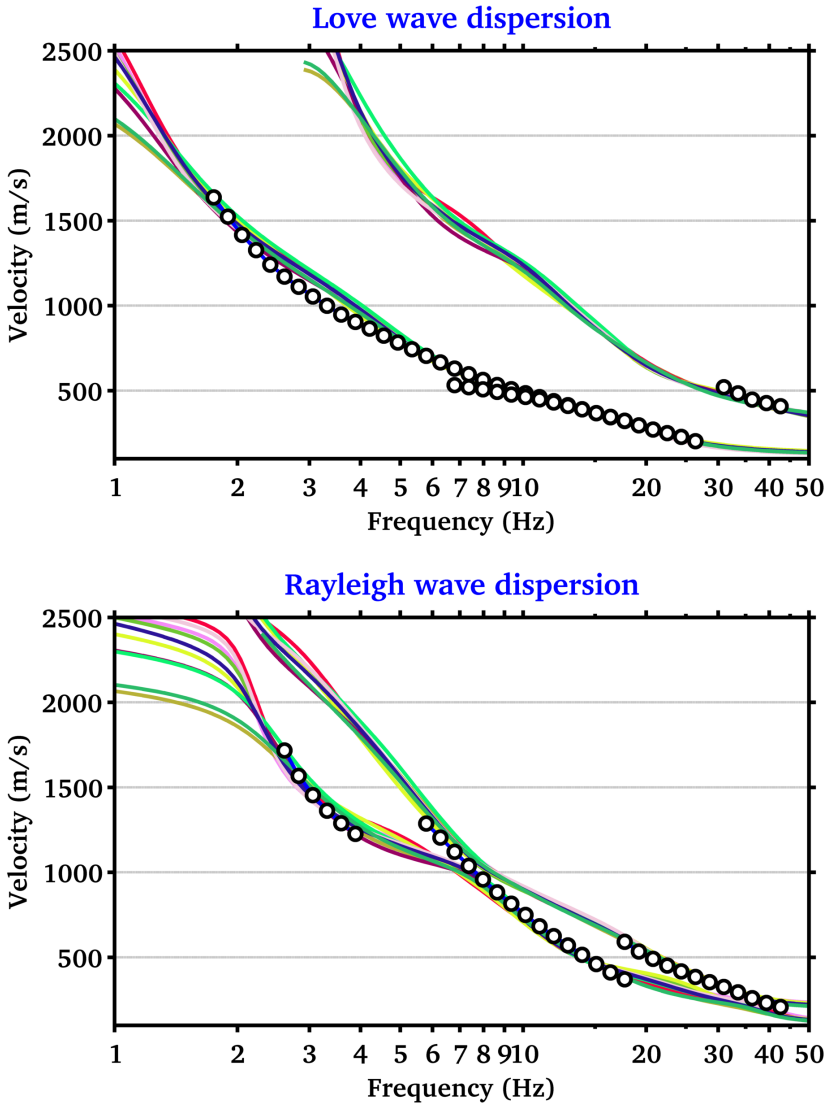

Figure 20 - *Dispersion curves computed from the best fitting models of the two proposed interpretation schemes (free and fix layers), compared with picked dispersion from active and passive seismic experiments.*

To parameterize the velocity model, two different approaches were implemented. The first one consisted in setting up an eight-layer model with fix interface depths. In such a case the free inversion parameters are then the velocities (P and S) and layer thicknesses. In the second case, a free-thickness layer approach was used. The advantage of the former method stays in the possibility to better resolve sharp velocity interfaces, while the second is less unique and better constraints the seismic velocity. The two approaches have to be nevertheless considered complementary, and they should provide consistent results.

Ten inversion tests (*runs*) were performed for each of the two model schemes, in order to minimize the effect related to a possible unfavorable initial randomization of the parameter space. The best fitting model from of each run was then collected (**Figure 19** and **Figure 22**) and used later on for the computation of the derived soil parameters.

In mode detail, the inverted velocity profiles (Vs and Vp) are gradient-like, but with at least two major interfaces, at about 40m and 200~300m. The first interface is actually constrained by high frequency part of the Rayleigh and Love dispersion curves (including higher modes from active surface wave analysis, **Figure 20**), which also gives good resolution on the uppermost portion of the velocity profile. The second boundary (less resolved) is solely controlled by the use of f_0 form H/V spectral ratios (**Figure 21**), and shows a considerable scatter. By considering the minimum available frequency of the surface-wave analysis, and by analyzing the scattering of the inverted models (**Figure 22**), it is realistic to assume the velocity profiles to be reliable down to a depth of about 200~350m. Below this value no direct constrain is available from data, and the velocity values are obtained by pure extrapolation.

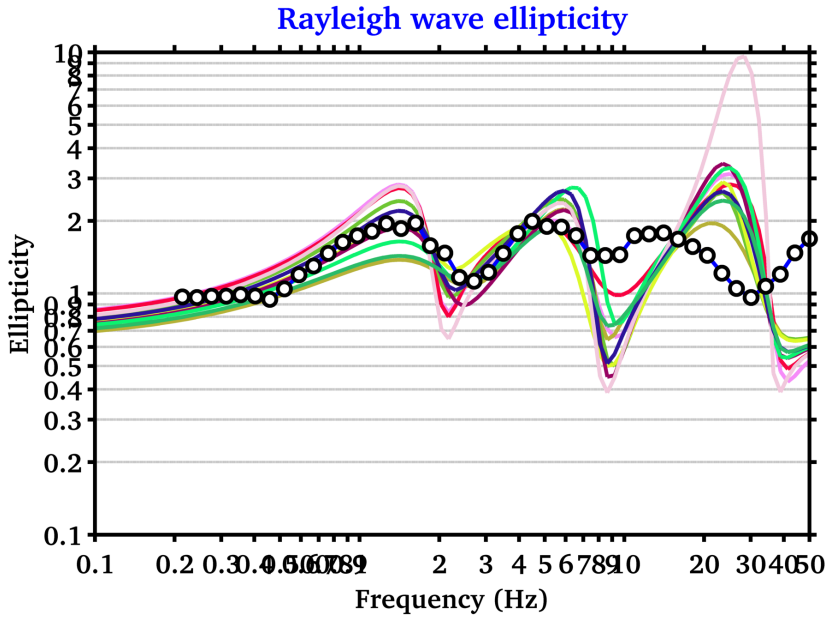

Figure 21 - *Rayleigh wave ellipticity curves computed from the best fitting models of the two proposed interpretation schemes (free and fixed layers), compared with average H/V spectral ratio from configuration R2 (scaled by sqrt(2)). The first two peaks are clearly reproducible, even though the H/V curve was not used during the inversion.*

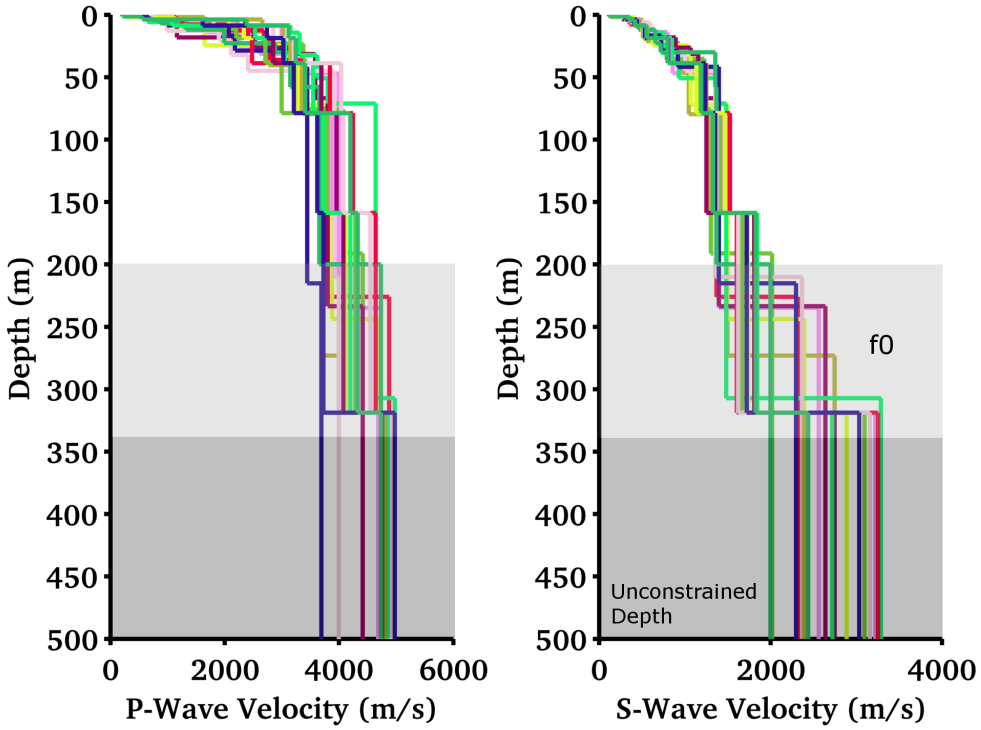

Figure 22 - *Comparison of all the best models from the two parameterization schemes (free and fixed layers). The two approaches produce consistent results. Depth range between about 200m and 350m is solely constrained by f_0 and should be considered approximately the maximum resolved depth.*

11. Engineering soil parameters

The ensemble of all the best inverted velocity profiles is then used to derive average soil parameters like the VsZ (average travel-time S-wave velocity over the depth Z, including Vs30, Table 1) and the quarter-wavelength (QWL) average velocities (Joyner et al., 1984) for a range of frequencies between 0.6 and 30Hz (**Figure 23**). The former is a standard parameter for the classification of ground-types in most building codes and in ground motion prediction equations. The latter is a parameter useful for the empirical estimation of the site-response and to assess the sensitivity of the seismic wave-field to the different depths. It has to be noticed that these two parameters are derived separately from all the best S-wave velocity models obtained from the inversion, and the results is finally averaged to improve statistics.

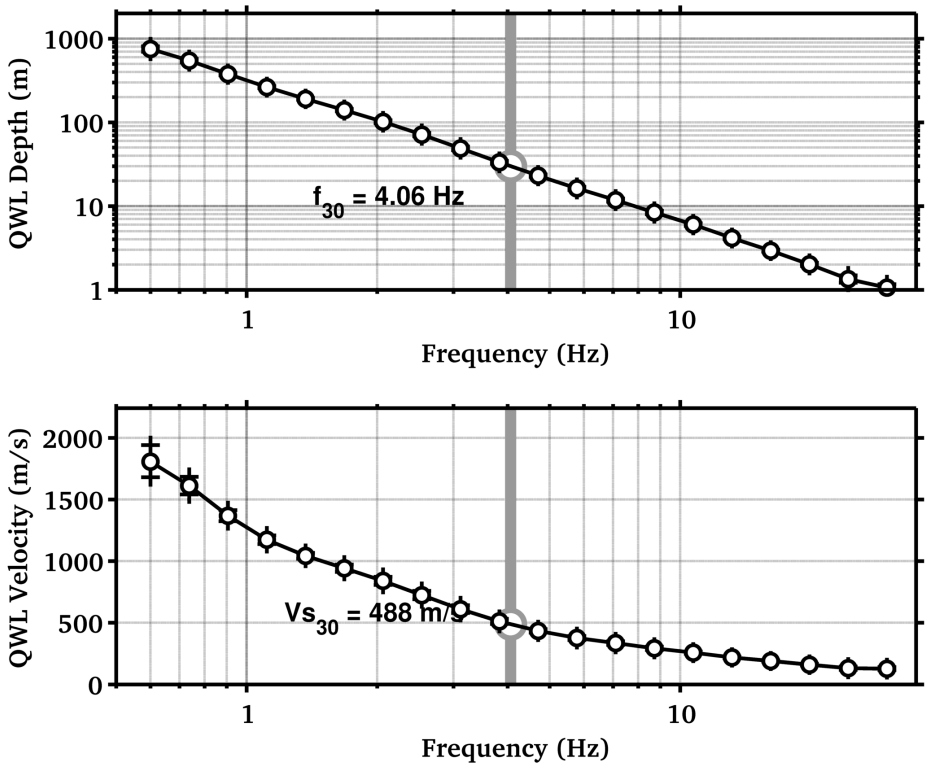

Figure 23 - *Quarter-wavelength representation of the inverted S-wave velocity profiles. Top: the depth-frequency dependency. Bottom: the QWL average velocity. The Vs30 value is indicated with its corresponding QWL frequency.*

12. Amplification models

Site amplification functions have been computed using two different approaches: the S-wave transfer function for vertical propagation and the quarter-wavelength amplification. In general the first method is used to evaluate the resonance characteristics of the site, while the second is more useful to assess the effect of the velocity contrasts between the lowermost rock layer (as reference) and the different QWL averaging depths. The two amplification functions are then corrected for the Swiss rock reference velocity profile as defined in Poggi et al. (2011), according to the procedure described in Edwards et al. (2013). Given the lower velocities in the uppermost part of the HAMIK profile compared to the Swiss reference, the final corrected amplification function shows a lower average amplification level at high frequencies than the uncorrected (**Figure 24**).

Averaging depth (m)	Vs-mean (m/s)	St.Dev.
5	238.32	3.71
10	314.41	8.61
15	365.85	9.92
20	407.07	9.40
25	450.41	7.92
30	**487.57**	**9.52**
40	552.09	15.62
50	616.39	16.86
75	738.90	21.16
100	834.85	20.56
150	962.88	21.21
200	1060.16	15.69

Table 1 - *Average travel-time velocities at different depths. Vs30 is highlighted.*

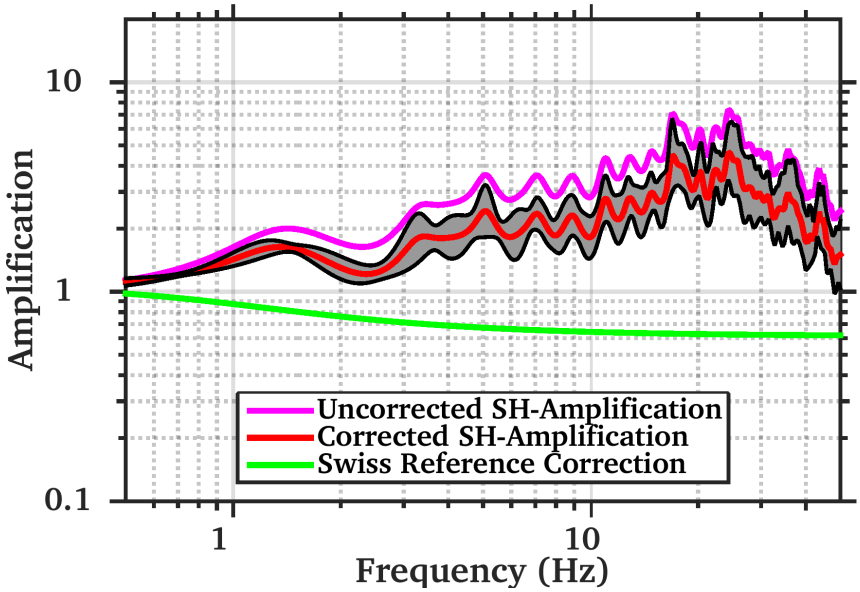

Figure 24 - *Correcting the SH-wave transfer function for the Swiss (rock) reference conditions (Poggi et al. 2011). The final corrected amplification function shows a lower (average) amplification at high frequencies than the uncorrected.*

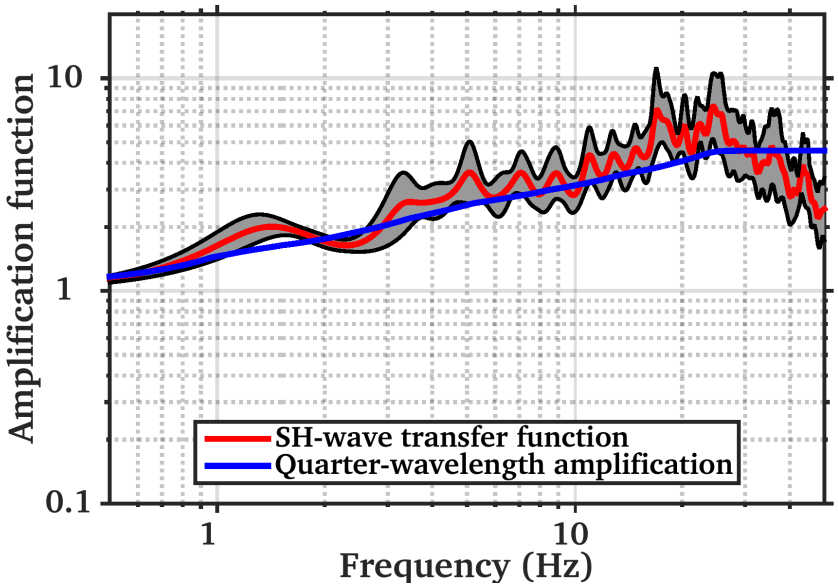

Figure 25 - *Comparison of amplification functions computed using the SH-wave transfer function and the quarter-wavelength formalism on the inverted velocity models.*

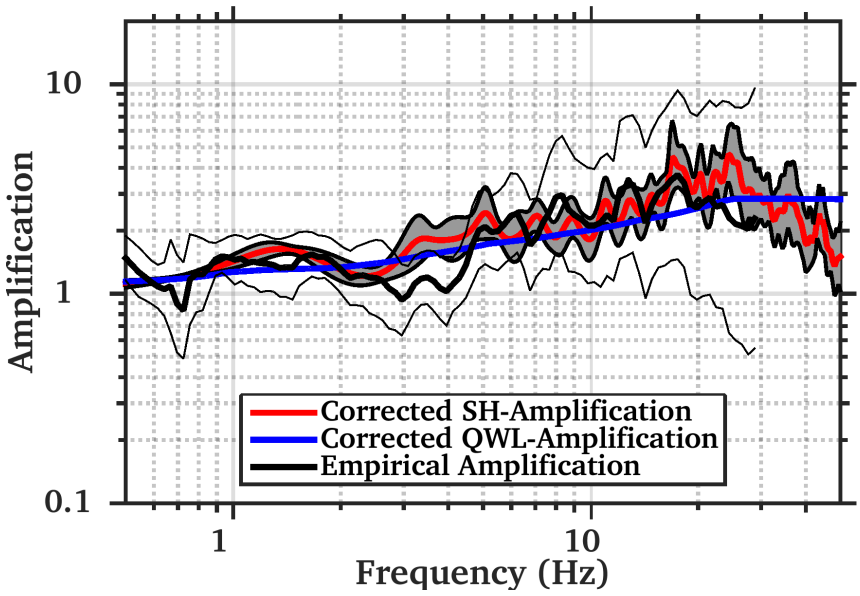

Figure 26 - *Comparison of amplification functions computed using the SH-wave transfer function and the quarter-wavelength approach with empirical observation from spectral modeling of low-magnitude earthquakes (here the anelastic spectrum). All functions are referenced to the Swiss rock reference model (Poggi et al. 2011).*

Amplification functions using the transfer function and the quarter-wavelength approach are comparable (**Figure 25**), even if the transfer function provides a slightly larger amplification, because of the presence of some weak resonance peaks. At low frequencies both methods converge to the same amplification level. It has to be notice that the amplification functions do not include attenuation at this stage of the analysis, as the quality factors of the site are too uncertain.

A good matching is obtained by comparison between the one-dimensional transfer function and the empirical amplification from spectral modeling of low-magnitude earthquakes as described in Edwards et al., 2013. However, the general trend is well reproduced by the analytical solution only when compared to the anelastic empirical amplification (**Figure 26**). The corresponding elastic function has low amplitude than the anelastic at high frequencies. This is likely due to a hill-constrained estimation of the attenuation operator *kappa* in presence of strong resonance peaks at high frequencies, which bias the fit of the attenuation decay function to be removed.

REFERENCES

Capon, J., 1969. High resolution frequency wavenumber spectrum analysis, Proc. IEEE, 57, 1408-1418.

Burjanek, J., G. Stamm, V. Poggi, J.R. Moore, and D. Fäh [2010], “Ambient vibration analysis of an unstable mountain slope”, Geophys. J. Int., Vol. 180, pp. 820-828.

Edwards, B., C. Michel, V. Poggi and D. Fäh (2013). Determination of Site Amplification from Regional Seismicity: Application to the Swiss National Seismic Networks. Accepted for publication in Seismological Research Letters.

Joyner, W. B., R. E. Warrick and T. E. Fumal (1981). The Effect of Quaternary Alluvium on Strong Ground Motion in the Coyote Lake, California, Earthquake of 1979, Bulletin of the Seismological Society of America, 71, 1333-1349.

Poggi, V., B. Edwards and D. Fäh (2011). Derivation of a Reference Shear-Wave Velocity Model from Empirical Site Amplification, Bulletin of the Seismological Society of America, 101, 258-274.

Poggi, V. and Fäh D., 2010. Estimating Rayleigh wave particle motion from three-component array analysis of ambient vibrations. Geophys. J. Int., 180-1, 251-267.